A NEW METHOD FOR SUPPRESSING OPTICAL TURBULENCE IN VIDEO

Dalong Li[†]*, Russell M. Mersereau*[†]*, David H. Frakes*[§] *and Mark J. T. Smith*[‡]

[†]School of ECE, Georgia Institute of Technology
Atlanta, GA, 30332, USA
{dalong,rmm}@gatech.edu

[§] 4-D Imaging, Inc
Atlanta, GA, 30332, USA
dave@bme.gatech.edu

[‡]School of ECE, Purdue University
West Lafayette, Indiana, 47907, USA
mjts@purdue.edu

ABSTRACT

The presence of optical turbulence in video acquired by cameras viewing scenes at long distances can contribute significantly to degradation. This problem arises routinely, for example, in astronomy where objects of interest reside beyond the earth's atmosphere. Optical turbulence introduces time-varying perturbations in the images as well as blurring. In this paper, we introduce a method for suppressing the effects of this turbulence to enhance the quality of the observed objects and scenes. The proposed method is based on a new form of adaptive control grid interpolation in which computed motion vectors are used as the basis for turbulence estimation and suppression. In particular, the quasi-periodicities of the turbulent motion are exploited in the algorithm, which allow them to be suppressed while true motion (such as panning and zooming) is preserved.

1. INTRODUCTION

Atmospheric turbulence in the air can often result in optical distortions that are visible in video acquired by cameras viewing scenes at long distances [1]. This phenomenon can be observed, for example, by looking at the cosmos through a telescope. The viewer observes planetary and stellar objects that appear to waiver. Another example of turbulence effects is the rippling wavy distortion that arises when observing a plane on a heated tarmac at the airport during a hot day. This turbulence has been studied by a number of authors [1, 2, 3, 4, 5, 6]. It is caused primarily by refraction index fluctuations from hot moving air currents, which perturb the incident wave fronts of reflected light. The dynamics surrounding these air currents are multifaceted and involve wind velocity, temperature, elevation, and sun intensity to mention a few. Optical turbulence suppression has been considered from the viewpoint of modeling the physical processes that produce the distortion and then employing the physical model to mitigate optical distortions. However, this is not is practical in many situations, since local atmospheric condition data are often not available. Clearly, there is value in an approach that addresses this problem without the need for atmospheric measurements. The approach taken here is to exploit the property that turbulent motion is spatio-temporally quasi-periodic and that the magnitude of the motion variation is modest.

We start by assuming that the turbulence-degraded video g can be modeled approximately as:

$$g(i,j,t) = D[x(i,j,t) * h(i,j,t),t] + \quad (i,j,t), \qquad (1)$$

where * denotes two-dimensional convolution, denotes time-varying additive noise, D denotes the turbulence induced time-varying geometric distortion, h is dispersive distortion component of the atmospheric turbulence, g is the observed degraded video, and x is the original video. When t is fixed at a time when $D(x) = x$ (i.e. no geometric distortion), the above model reduces to the familiar degradation model:

$$g(i,j) = x(i,j) * h(i,j) + \quad (i,j). \qquad (2)$$

Much of the previous work in turbulence-degraded image restoration has focused on still images and thus has only treated time invariant distortion [1, 2, 4]. Few have considered addressing the geometric distortion component D. Since the optical distortion is not known exactly because of the random nature of the turbulence, the problem was treated as a blind image deconvolution problem in [4]. A few authors have considered methods based on image registration and warping techniques [5, 6] in which the time varying nature of turbulence is addressed explicitly. For example, a hierarchically-windowed cross-correlation technique is used in [5] to register each pixel in each image in a time sequence to a corresponding point in a prototype image, to sub-pixel accuracy. The prototype is formed initially by simple averaging of the image sequence. Then it is updated by the averaging of the processed image sequence. Another example is the adaptive control grid interpolation used in [6] for image registration. This method was shown to work quite well when in the absence of real motion. Not only did the restored video have higher resolution, but the video was stabilized and the turbulence-induced distortion was suppressed. The notable shortcoming of these methods is that it can not handle the situation in which both turbulence and real motion are present. While using time-averaged frames as reference frames can address turbulence, such an approach destroys any true motion that might be present. These approaches are thus unable to handle situations involving panning, zooming, or object movement. The new method presented in this paper is able to handle all of the above.

In this paper, we present an algorithm to compensate for the time-varying distortion D by exploiting the quasi-periodicities in the motion field. Control grid interpolation [6, 11] is used to produce the motion field between images. Trajectories of the pixels are computed from the motion fields. Within this domain, the turbulent and real motion trajectories can be separated as detailed in next section.

The reminder of the paper is organized as follows. In Section 2, the details of the algorithm are given. In Section 3, the implementations and the experimental results of our approach are reported, followed by conclusions in Section 4.

2. THE SUPPRESSION ALGORITHM

The proposed algorithm can be viewed as having three distinct components: compensation of the dispersive distortion

h; modeling of the motion; and compensation of the motion-induced distortion.

2.1 Compensation of h

Given g, our first step is to compensate for h at each frame. The optical transfer function (OTF) of atmospheric turbulence can be modeled as

$$H(u,v) = e^{-\ (u^2+v^2)^{5/6}}, \tag{3}$$

where controls the severity of the blur [7]. The severity of the OTF increases as increases. With this model of the OTF, estimation of h reduces to determining the parameter . A number of approaches can be used to estimate . Two notable examples include maximum likelihood [9] and generalized cross validations [8]. Both of those use an autoregressive moving average (ARMA) model, in which the image is modeled as an autoregressive process and the OTF is modeled as a moving average process. In this work, we obtain by minimizing the Kurtosis [10]. Kurtosis can be used as a measurement of the quality of the deblurred image. For each in the given search space , H can be obtained by the equation (3) and the compensated still frames g_t can be computed via the Wiener filter:

$$G_t(u,v) = \frac{H^*(u,v)X(u,v)}{|H(u,v)|^2 + P\ (u,v)/P_x(u,v)}, \tag{4}$$

where P_x and P are the power spectral density of the signal and noise, respectively. Since x is not available, P_x is approximated by P_g. P is estimated in the frequency domain.

The kurtosis of the restored image is computed and used as a measurement of the fitness of the . Then the with the minimal kurtosis is selected as the estimation of the parameter and the corresponding restored image is used as the estimation of x. Each frame is deblurred separately in the video.

Thus in this step, we have compensated for the dispersive distortion, resulting in a new video sequence. To suppress noise which is often present in the resulted new video sequence, the average is taken of the current frame, the previous warped to the current frame, and the next frame warped to the current frame.

2.2 Modeling of the motion

The remaining step is to compensate for the geometric distortion D. For this component, we use a modified control grid interpolation (CGI) representation [6]. The motion field is obtained by segmenting the image into small contiguous square regions. The corners of these regions form control points, which are used as the anchors from which the intermediate motion vectors are derived using bilinear interpolation. CGI is attractive for this application because it allows for the representation of complex non- translational motion and in that regard is significantly different from the conventional block matching algorithm. We use a high resolution CGI algorithm with embedded optical flow equations for calculating the motion of the control points, leading to an accurate dense motion field representation. Figure 1 shows an example of the motion field in a region of turbulence, where the magnitudes have been scaled for visualization purposes.

Within each region, the relationship between pixels in images I_0 and I_1 is described by Equation (5). In Equation

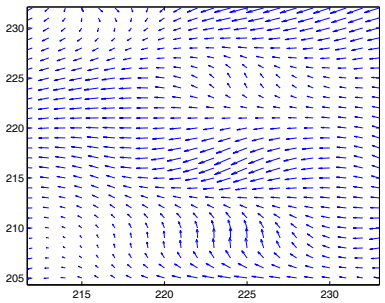

Figure 1: Example of a turbulent motion field.

(5) $d_1[i,j]$ is the horizontal component of the displacement vector at spatial location (i,j) and $d_2[i,j]$ is its vertical component. This is equivalent to finding the optimal motion vectors at each of the control points on the border of the region.

$$\begin{aligned} I_1[i,j] &= I_0[i+d_1[i,j], j+d_2[i,j]] \\ d_1[i,j] &= {}_1 + {}_2 i + {}_3 j + {}_4 ij = {}^T [i,j] \\ d_2[i,j] &= {}_1 + {}_2 i + {}_3 j + {}_4 ij = {}^T [i,j] \end{aligned} \tag{5}$$

A quadtree is used to segment the image into rectangular regions R . The bilinear parameters , are found in each region R by minimizing the quantity

$$\sum_{[i,j]\in R} (I_0[i,j] - I_1[i + {}^T [i,j], j + {}^T [i,j]])^2 \tag{6}$$

By using a first-order Taylor series approximation in which all higher order terms have been discarded, the error function in Equation (6) reduces to

$$\sum_{[i,j]\in R} (I_0[i,j] - I_1[i,j] - \frac{I_1[i,j]}{i} {}^T [i,j] - \frac{I_1[i,j]}{j} {}^T [i,j])^2 \tag{7}$$

The accuracy of the estimates is increased by changing the location of the Taylor series approximation from (i,j) to $(i + {}^T [i,j], j + {}^T [i,j])$ and updating the parameter estimates. This process usually converges in fewer than five iterations.

2.2.1 *Trajectory estimation*

The motion computation is based on previous frame so that the system is causal. To compute the motion trajectories, we denote the motion between frame t and frame $t-1$ as $v_{t,t-1}(i,j)$. Once the motion between the frames has been computed, the trajectory for each pixel can be obtained. There are two methods that can be used to build the trajectory $T(i,j,t_0 : t_0 - n)$, where t_0 denotes the location of the starting frame. $T(i,j,k)$ represents the location of the start frame I_{t_0} pixel in frame k. Therefore, we have $T(i,j,t_0 : t_0 - n) = \{T(i,j,t_0), T(i,j,t_0-1), \ldots, T(i,j,t_0-n)\}$.

Given the transitional matrix of motion fields $\{v_{t_0,t_0-1}(i,j), v_{t_0-1,t_0-2}(i,j), \ldots, v_{t_0-n+1,t_0-n}(i,j)\}$, $T(i,j,t_0 : t_0 - n)$ can be computed iteratively as follows:

$$T(i,j,t_0) = (i,j)$$

$$\begin{aligned} T(i,j,t_0-1) &= T(i,j,t_0)+v_{t_0,t_0-1}(T(i,j,t_0)) \\ &\vdots \\ T(i,j,t_0-n) &= T(i,j,t_0-n+1) \\ &+ v_{t_0-n+1,t_0-n}(T(i,j,t_0-n+1)) \end{aligned} \tag{8}$$

The advantage of this approach is its computational efficiency. All of the motion fields except for the farthest one from the current frame (I_{t_0}), $v_{t_0-n+1,t_0-n}(i,j)$, can be used again when the current frame moves to the next frame I_{t_0+1} in the video. At each frame time, only one motion field needs to be computed to construct the new motion trajectory $T(i,j,t_0+1:t_0-n+1)$.

However, if noise is present the above approach will propagate errors, i.e. the error from $T(i,j,t_0+k)$ is passed to $T(i,j,t_0+k-1)$. As an alternative, we take the following approach. The transitional matrix is instead made up of motion fields $\{v_{t_0,t_0-1}(i,j), v_{t_0,t_0-2}(i,j),\ldots,v_{t_0,t_0-n}(i,j)\}$. With this choice, when the motion is computed, the source image remains fixed, while the target image is changed.

$T(i,j,t_0:t_0-n)$ is computed by the equations:

$$\begin{aligned} T(i,j,t_0) &= (i,j) \\ T(i,j,t_0-1) &= (i,j)+v_{t_0,t_0-1}(i,j) \\ &\vdots \\ T(i,j,t_0-n) &= (i,j)+v_{t_0,t_0-n}(i,j) \end{aligned} \tag{9}$$

Although the error-propagation problem is prevented, the computation is greatly increased since the source frame shifts and each motion field needs to be recomputed when the current frame advances to the next one.

2.2.2 Compensation of motion induced distortion

For turbulence, which is quasi-periodic, the net displacement over the duration of a period is approximately zero. For real motion, this will not be the case. Consequently, we can suppress the turbulence by using the centroid of the trajectory taken over a period.

$$\hat{T}(i,j) = \frac{1}{n+1}\sum_{t_0-n\le k\le t_0} T(i,j,k) \tag{10}$$

$\hat{T}(i,j)$ approximates the locations of the pixel in frame t_0 without the turbulence distortion. We then warp the pixels in frame t_0 from its original location toward the estimated location. The quasi-periodicities of the turbulence are suppressed by this process while other motion characteristics are preserved. When no real motion is present, it is advantageous to increase n so that more turbulence motion will be smoothed. However, when real motion exists, as you increase n, the motion between the frames will be large and it will be difficult to reliably compute the motion. Thus the trajectory will contain lots of error and the overall performance is decreased.

3. EXPERIMENT

3.1 Real turbulence-degraded video

A number of naturally acquired videos were tested that contained real atmospheric turbulence. Figure 2 shows an example of a frame taken from a video sequence of the moon acquired through a telescope. The sequence contains a fair amount of jitter, time-varying geometric distortion, and blurring. Visual inspection of the processed video shows noticeable reduction in the distortion. The jitter and geometric distortions are no longer visible, and the image is noticeably sharper. The only pixel variations one observes is random pixel intensity fluctuations. Ideally, one would expect that each frame would be identical. Because of noise and compensation errors, the ideal is not quite achieved, although results look very good. The mean-square-error between successive frames is shown in Figure 3 for both the original turbulent sequence and the enhanced sequence. While the plots reveal both sequences contain frame differences, the variations in these differences are dramatically reduced for the processed sequence.

3.2 Simulated turbulence-degraded video

It is important for evaluation purposes to have optical turbulence examples with ground truth. Thus, we generated a number of simulated optical turbulence examples that also included real motion. To create the simulated examples, we use the OTF in equation (3) to simulate h in equation (1). D is simulated by the motion fields $\{v_{t-1,t}(i,j) : t \in [2,l]\}$ (l is the length of the video) computed from the real turbulence video sequences. The noise is assumed to be white. Since turbulence blurring is time varying, s were chosen by comparison with the real turbulence-degraded images. We adjusted the on a frame by frame basis to match the distortion observed in the real data. Noise variances were chosen from the set $\{0.0010, 0.0015, 0.0020, 0.0025, 0.0030\}$ to simulate time varying Gaussian noise of the type encountered in our real data sets. We applied the degradations to a video sequence taken at a parking lot while a car was exiting in front of a building.

Kurtosis minimization was used to estimate in the deblurring phase of the process. Then, the images were deblurred using equation (4). Noise in the deblurred images are removed as described in section 2.1. The geometric distortion was suppressed using equations (9) and (10) as described in section 2.

Since the true video is available, we can compute the PSNR to measure the restoration performance. For comparison, we also implemented the time-averaging reference frame approach used in [5, 6]. That is, the video is filtered by a moving averaging filter of length 5 to form the reference sequence. Then the frames are registered to the reference frames. Since there is a moving object in the video, the time-averaged reference frames led to poor results, as shown in Fig. 4. The proposed method performs noticeably better than the time averaged reference approaches both subjectively and in terms of PSNR.

A visual example of the geometric distortion suppression is highlighted in Fig. 5. The horizontal line of the window frame are clearly distorted in the original, but corrected in the enhanced version.

4. CONCLUSIONS AND REMARKS

The new algorithm attempts to address both the geometric and dispersive components of atmospheric distortion. The visual improvement obtained is dramatic. A key issue we are currently investigating is modeling the quasi periodicities of the turbulence. These geometric fluctuations are localized

with different periods. Further improvement should be possible by linking the centroid calculations to model estimates of the local turbulent periodicities. The new algorithm has the distinct advantage of being able to handle natural motion, including panning and zooming. Thus, we envision this approach to be potentially useful in astronomy and for a variety of long distance surveillance applications.

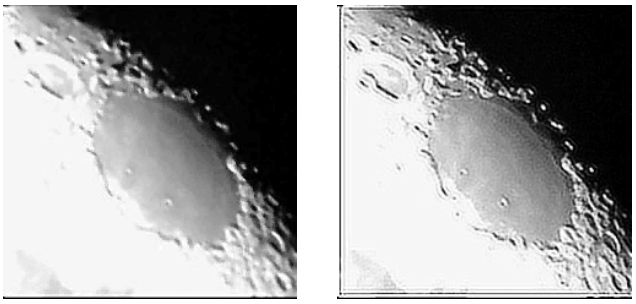

(a) (b)

Figure 2: (a) Real atmospheric turbulence blurred image and (b) the processed one.

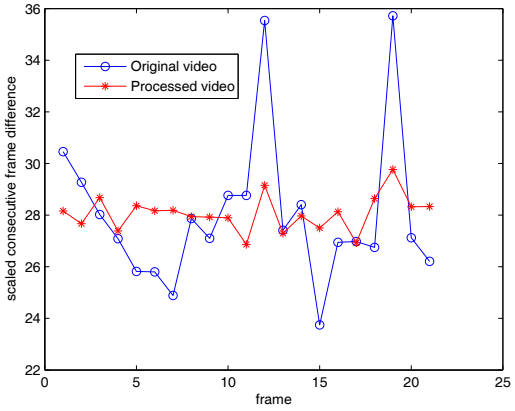

Figure 3: Mean-square-error between consecutive frames in the original video and processed video.

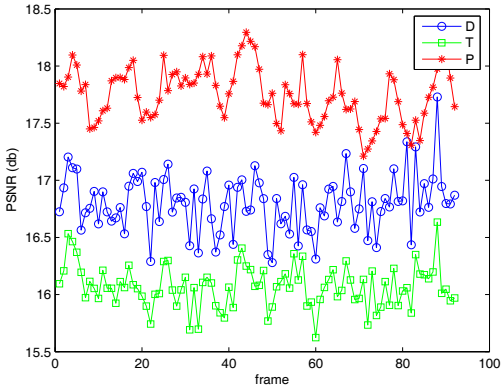

Figure 4: PSNR comparison of proposed algorithm with time-averaging reference [5, 6]. D: the degraded video; T: time-averaging and dewarp method; P: proposed algorithm.

(a) (b)

Figure 5: (a) Degraded frame and (b) Restored frame in the simulated video.

REFERENCES

[1] D. G. Sheppard, B. R. Hunt and M. W. Marcellin, "Iterative multiframe super-resolution algorithms for atmospheric turbulence-degraded imagery," in *Proc. ICASSP 1998*, Seattle, WA, USA, May. 12-15. 1998, pp. 2857 –2860.

[2] C. Bondeau and E. Bourennane, "Restoration of images degraded by the atmospheric turbulence," in *Proc. ICSP 1998*, Beijing, China, Oct. 12-16. 1998, pp. 1056–1059.

[3] M. C. Roggemann and B. Welsh, *Imaging Through Turbulence*. CRC Press, 1996.

[4] T. J. Schulz, "Multi-frame blind deconvolution of astronomical images," *Journal of the Optical Society of America A* , vol. 10, pp. 1064–1073, 1993.

[5] D. Fraser, G. Thorpe and A. Lambert, "Atmospheric turbulence visualization with wide-area motion-blur restoration," *Journal of the Optical Society of America A* , vol. 16, No.7, pp. 1751–1758, July. 1999.

[6] D. H. Frakes, J. W. Monaco and M. J. T. Smith, "Suppression of atmospheric turbulence in video using an adaptive control grid interpolation approach," in *Proc. ICASSP 2001*, May. 7-11. 2001, pp. 1881–1884.

[7] R. E. Hufnagel and N. R. Stanley, "Modulation transfer function associated with image transmission through turbulence media," *Journal of the Optical Society of America A* , vol. 54, pp. 52–61, 1964.

[8] S. J. Reeves and R. M. Mersereau, "Blur identification by the method of generalized cross-validation," *IEEE Trans Image Processing*, vol. 1, pp. 301–311, July. 1992.

[9] R. L. Lagendijk, A. M. Tekalp and J. Biemond, "Maximum likelihood image and blur identification: a unifying approach," *Optical Engineering*, vol. 29, pp. 422–435, May. 1990.

[10] D. Li, R. M. Mersereau and S. Simske, "Blur identification based on kurtosis minimization," *to be published in Proc. ICIP 2005*.

[11] G. J. Sullivan and R. L. Baker, "Motion compensation for video compression using control grid interpolation ," in *Proc. ICASSP 1991*, pp. 2713–2716.